Hippocampus

WILEY

RESEARCH ARTICLE

Pharmacological Profile of Early Sharp Waves in the Neonatal Rat Hippocampus

Dmitrii Shipkov[1,2] | Daria Vinokurova[1] | Karina Tukhvatullina[1] | Guzel Valeeva[1]

[1]Laboratory of Neurobiology, Kazan Federal University, Kazan, Russia | [2]Okinawa Institute of Science and Technology, Okinawa, Japan

Correspondence: Guzel Valeeva (gurvaleeva@kpfu.ru)

Received: 6 May 2025 | **Revised:** 10 March 2026 | **Accepted:** 9 April 2026

Keywords: AMPA | early sharp waves | GABA | hippocampus | neonatal rat | NMDA | receptors

ABSTRACT

Early activity patterns support the development of neuronal networks by promoting synaptic plasticity. In the hippocampus of neonatal rats and mice in vivo, early sharp waves (eSPWs) are the first pattern of synchronized network activity. The activation of glutamate- and GABA(A)-mediated synaptic currents was described during eSPWs. However, the contribution of different receptor subtypes to eSPW generation is still obscure. To explore the receptor mechanisms of eSPW generation we used a «superfused hippocampus» preparation, which allows a drug application directly to the large area of the hippocampal surface in vivo. Using silicon probe recordings from the superfused hippocampus of neonatal Wistar rats, we assessed electrophysiological properties of eSPWs in control conditions and during the superfusion with glutamate and GABA receptor antagonists. We showed that blocking the AMPA/kainate and NMDA glutamate receptors reduced to a different degree the eSPW frequency and neuronal firing associated with eSPWs. Only when applied simultaneously did the AMPA/kainate and NMDA receptor antagonists completely suppress eSPWs. At the same time, GABA(A) receptors appeared to have a limited role in eSPW generation as eSPWs persisted after GABA(A) receptor blockade alternating with recurrent epileptiform discharges; yet, eSPW amplitude was reduced after epileptiform activity onset. We also observed no changes in eSPW properties produced by blocking the GABA(B) receptors. Taken together, our findings reveal a predominant involvement of AMPA/kainate and NMDA glutamate receptors in eSPW generation and emphasize the role of eSPWs in providing conditions for NMDA receptor-mediated plasticity in the developing hippocampus.

1 | Introduction

During early development, neuronal networks of the brain are characterized by the presence of intermittent correlated activity bursts. These early activity patterns provide synaptic plasticity in the developing circuits, participating in this way in the formation of specific connections between neurons (Katz and Shatz 1996; Griguoli and Cherubini 2017; Cossart and Khazipov 2022). In the developing hippocampus in vivo, the first organized network activity pattern is early sharp waves (eSPWs) (Leinekugel et al. 2002; Karlsson et al. 2006; Mohns et al. 2007; Valeeva, Janackova, et al. 2019; Valeeva, Nasretdinov, et al. 2019; Graf et al. 2021; Cossart and Khazipov 2022; Juzekaeva et al. 2024). The eSPWs appear in the neonatal rat and mouse hippocampus starting from 1 to 2 days after birth to be most pronounced throughout the first postnatal week. The electrographic pattern of eSPWs resembles that of sharp wave—ripples (SPW-Rs) observed in adult hippocampus and characterized by a negative local field potential (LFP) peak in CA1 *str. radiatum* and LFP polarity reversal just below the pyramidal cell layer. Both neonatal and adult forms of SPWs are accompanied by neuronal firing and activation of glutamatergic and GABAergic signaling in the pyramidal cell layer (Leinekugel et al. 2002; Hajos et al. 2013; Schlingloff et al. 2014). At the same time, eSPWs lack the ripple oscillations characteristic of SPW-Rs (Ylinen et al. 1995; Leinekugel et al. 2002; Buhl and Buzsáki 2005;

Pochinok et al. 2024). Also, the eSPW generation is associated with spontaneous myoclonic body movements and concomitant activation of inputs from entorhinal cortex (Karlsson et al. 2006; Mohns et al. 2007; Valeeva, Janackova, et al. 2019) in contrast to SPW-Rs generated autonomously within the CA3–CA1 hippocampal network (Buzsáki et al. 1983; Csicsvari et al. 2000; Wu et al. 2005; Ellender et al. 2010; Sullivan et al. 2011). It remains unknown, however, whether eSPWs exhibit different synaptic receptor mechanisms as well.

Numerous pharmacological studies have described an essential role of AMPA/kainate glutamate receptors and GABA(A) receptors in the generation of SPW-Rs, and the majority of these studies have been performed in vitro (Papatheodoropoulos and Kostopoulos 2002; Maier et al. 2003; Wu et al. 2005; Behrens et al. 2005; Ellender et al. 2010; Papatheodoropoulos 2010; Hofer et al. 2015). As for eSPWs, this activity pattern was never observed in hippocampal slice preparation. Instead, neonatal hippocampal slices of mice and rats generate giant depolarizing potentials (GDPs) considered to be an in vitro counterpart of eSPWs (Leinekugel et al. 2002; Buzsáki 2015; Cossart and Khazipov 2022). AMPA and GABA(A) receptor-mediated conductances are known to be crucial for GDP generation (Ben-Ari et al. 1989; Strata et al. 1997; Bolea et al. 1999; Valeeva et al. 2010), and GABA(B) receptors have been shown to participate in GDP termination (Khalilov et al. 2017). Glutamatergic NMDA receptors contribute to the SPW-Rs and GDPs patterning as well (Khazipov et al. 1997; Leinekugel et al. 1997; Colgin et al. 2005; Ellender et al. 2010; Papatheodoropoulos 2010), however, their activation is not substantial for both activity patterns generation (Bolea et al. 1999; Maier et al. 2003; Behrens et al. 2005; Wu et al. 2005; Hofer et al. 2015). While considered for a long time as homologous activity patterns, eSPWs and GDPs differ in their dependence on intracellular chloride concentration set by NKCC1 cotransporter (Pfeffer et al. 2009; Murata and Colonnese 2020; Graf et al. 2021), as well as in their generative network mechanisms (Juzekaeva et al. 2024), suggesting that other differences in hippocampal in vitro and in vivo early activity patterns may also exist.

Bursts of glutamatergic and GABAergic synaptic currents associated with eSPWs were described in the developing rat hippocampus in vivo (Leinekugel et al. 2002). However, the contribution of defined receptor subtypes (AMPA/kainate, NMDA, GABA(A), and GABA(B) receptors) to eSPW generation remains unexplored. To investigate this issue, we used a «superfused hippocampus» technique for application of specific receptor blockers to the dorsal hippocampus of neonatal rats in vivo. It allows relatively local pharmacological manipulations that avoid systemic effects. This technique was originally described to record pharmacologically induced epileptiform activity from the CA3 hippocampal area of 2–3 weeks old rats (Khazipov and Holmes 2003). We have adapted the technique for the recording of physiological activity in the CA1 hippocampus of postnatal days (P) 5–7 rats. In our silicon probe recordings from superfused hippocampus preparation, eSPWs were observed under control conditions and during 1–1.5 h of drug application via superfusion. We used receptor antagonists to uncover a contribution of GABA and glutamate receptors activated by physiological concentrations of endogenously released neurotransmitters to eSPW generation. Assessing the changes in electrophysiological features of eSPWs caused by receptor antagonists, we found the predominant significance of glutamatergic over GABAergic conductances and the importance of NMDA receptors for eSPWs generation in neonatal rat hippocampus in vivo.

2 | Methods

2.1 | Animal Preparation

Wistar rats of both sexes from postnatal days (P) 5–7 were used (53 rat pups in total). Preparation of the animals for head-restrained recordings was performed under isoflurane anesthesia (4% for induction, 1.5%–2.5% for maintenance). The skull of the animal was cleaned of skin and periosteum using Hemostab $AlCl_3$ solution (Omega Dent, Russia), dried, and covered with a thin layer of cyanoacrylate glue and self-curing acrylic denture repair material (Meliodent RR, Kulzer, GmbH, Germany), leaving the surface of one or both parietal bones open. At the end of the surgery, animals were injected intraperitoneally with 15% urethane solution (1.5 g/kg, Sigma-Aldrich, USA). A metal ring was fixed to the skull by dental cement and via ball-joint to a magnetic stand. For standard hippocampal recordings, a hole with a diameter of about 0.2 mm was made in the bone above the dorsal hippocampus, where a recording probe was subsequently installed using stereotaxic coordinates (Khazipov et al. 2015). For superfused hippocampus recordings, the round portion of parietal bone (~3 mm diameter) above the dorsal hippocampus was removed, and the underlying neocortex was gently aspirated and replaced by cylindrical polymeric chamber (OD 3 mm, ID 2 mm, 2 mm height) with a mesh bottom (Figure 1A). The chamber was positioned 1 to 4 mm mediolaterally and 0.5–3.5 mm posterior to bregma, except for experiments with electrical stimulation of angular bundle, where the chamber was positioned 1 mm more posteriorly to allow space for the stimulating electrode. In the latter case, the recording coordinates remained unchanged. The neocortex was removed with great care to keep the hippocampal *str. oriens* intact so that even corpus callosum fibers lying between the neocortex and hippocampus remained unaffected in some animals. Top edge of the chamber was hermetically fixed to the bone using cold cure acrylic. A fine bar thermocouple (Omega Engineering, CT, USA), perfusion inlet and outlet tubes (0.45 mm diameter) were placed within the chamber. Inside the chamber, the hippocampal surface was continuously perfused (0.8–1.5 mL/min) with an artificial cerebrospinal fluid (ACSF) of the following composition (in mM): NaCl 126, KCl 2.5, $CaCl_2$ 2.0, $MgCl_2$ 1.0, $NaHCO_3$ 21.4, NaH_2PO_4 1.7, glucose 11 (pH 7.4). The ACSF temperature was maintained at 32°C–34°C using an automatic temperature controller (Warner Instr., USA). The thermocouple voltage data were recorded throughout the experiment to control ACSF temperature fluctuations in the chamber, which did not exceed 1°C–2°C during the entire recording.

2.2 | In Vivo Electrophysiology

Extracellular recordings of local field potentials (LFP) and multiple unit activity (MUA) were performed along the CA1–dentate gyrus axis of dorsal hippocampus using DiI (Sigma-Aldrich,

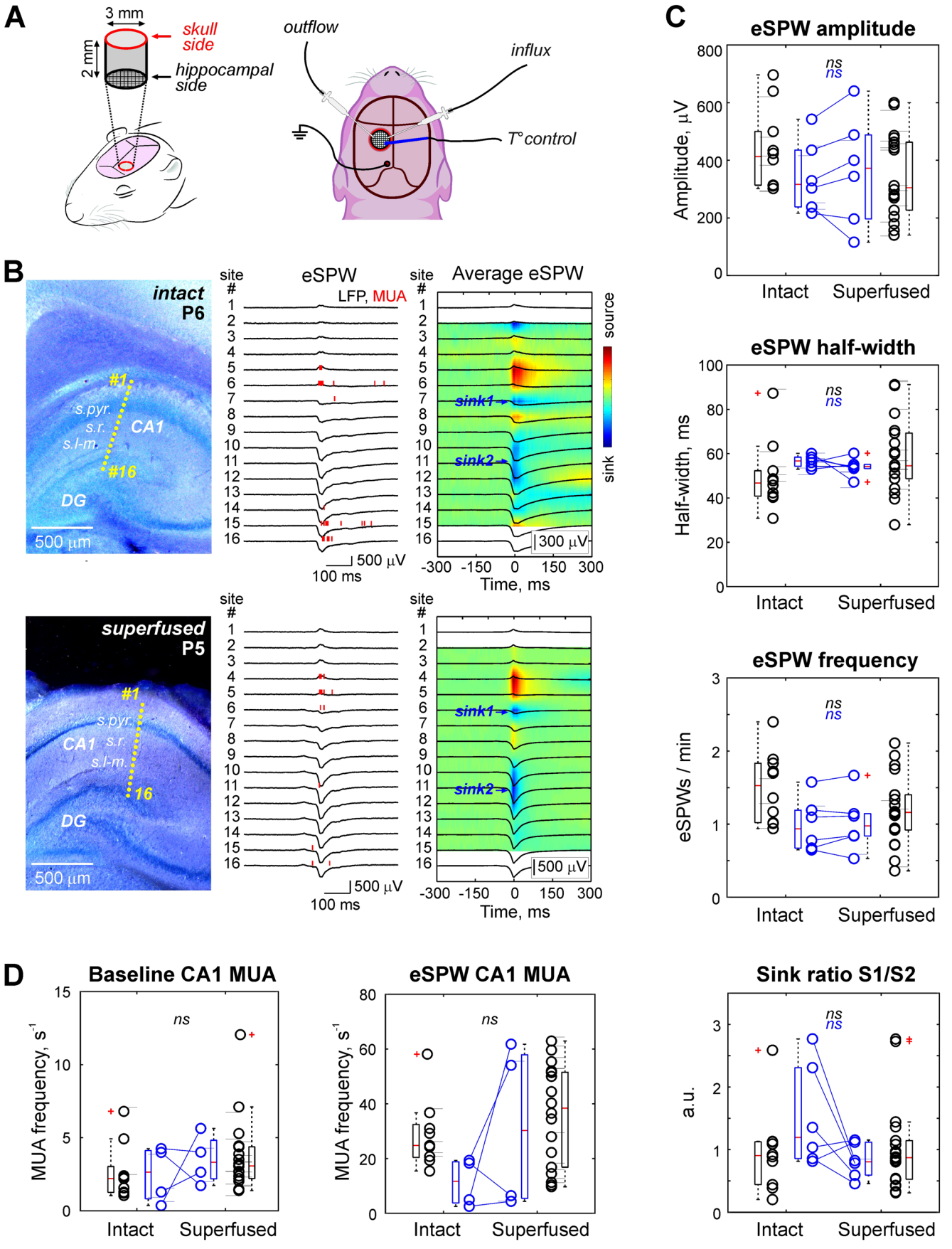

FIGURE 1 | Legend on next page.

FIGURE 1 | Electrophysiological properties of early sharp waves (eSPWs) in the intact and superfused hippocampi of neonatal rats in vivo. (A) A schematic illustration of unilateral superfused hippocampus preparation setup including the cylindrical superfusion chamber with a mesh bottom (shown on the left above the opening in the left parietal bone), influx and outflow tubes and fine thermocouple probe. (B) The microphotographs of cresyl violet stained slices of intact and superfused hippocampi of P6 and P5 rat pups with a reconstruction of recording sites location (left panels), examples of individual eSPWs recorded using 16-channel silicon probe (middle panels) from intact and superfused CA1 hippocampi and average eSPWs overlaid on current-source density maps (right panels). *s.pyr.*—stratum pyramidale, *s.r.*—stratum radiatum and *s.l-m.*—stratum lacunosum moleculare of CA1 hippocampus. Red bars above the local field potential (LFP) traces on middle panels indicate multiple unit activity (MUA) on corresponding channels. (C) Group data on eSPW amplitude, half-width, frequency and sink ratio in the intact and superfused hippocampi of P5-7 rats. The boxplots show a median (center line), Q1 and Q3 quartile values (edges), non-outlier extremes (whiskers) and outliers ('+' marker symbols). (D) Group data on MUA baseline frequency (left) and MUA frequency within [−50; 100] ms interval around eSPW peak in CA1 pyramidal cell layer of 9 intact and 18 superfused hippocampi of P5-7 rats. Each pair of connected circles on (C) and (D) shows eSPW property values in the intact and superfused hippocampi of one individual rat pup, and unconnected circles indicate eSPW property values in the intact and superfused hippocampi of different rats. ns—non-significant.

USA) coated 16-channel silicon probes with 50 μm separation distance between the electrodes (NeuroNexus, USA). A silver chloride wire placed in the parietal cortex served as a ground electrode. During the recording, animals were surrounded with a cotton nest and heated via thermal pad (35°C–37°C, Warner Instr., USA). To evoke hippocampal responses, angular bundle fibers were electrically stimulated (50 μs, 50–65 V, 1/20 s) using a bipolar tungsten electrode (Microelectrodes Ltd., UK). The stimulating electrode location was 500–600 μm posterior to the recording site. Signals from extracellular recordings were amplified and filtered (1000×; 0.15 Hz–9 kHz) using Digital Lynx SX amplifier (Neuralynx, USA), digitized at 16–32 kHz.

2.3 | Histology

After recordings, the animals were deeply anesthetized with isoflurane (5%), and their brains were removed. The brains were fixed in 4% paraformaldehyde and 1% glutaraldehyde for 2 days, then rinsed in phosphate-buffered saline and cut into 100 μm-thick coronal slices using a vibratome (Thermo Fisher Scientific, MA, USA). The silicon probe location in the hippocampus was assessed through identification of the DiI track. Thereafter, DiI tracks were overlaid on the microphotographs of corresponding brain slices after cresyl violet staining. The recording site location was verified by the highest MUA rate in the CA1 pyramidal cell layer. The reconstructed site location was further used to identify which of the probe channels were in the *str. radiatum* and *str. lacunosum–moleculare* of hippocampus during recording. The location of both channels coincided with current sinks on current-source density (CSD) maps, and channels in *str. radiatum* exhibited the largest LFP amplitude during eSPWs.

2.4 | Data Analysis

Electrophysiological data were processed and analyzed in MATLAB (MathWorks, MA, USA) as described previously (Valeeva, Janackova, et al. 2019). Hippocampal eSPWs were detected semi-automatically from down-sampled (1000 Hz), bandpass filtered (3–100 Hz, Chebyshev Type 2 Filter) LFP signals. All troughs greater than 2–4 SD from the least active 100 s long epoch through the entire record were first detected from the channel located in the *str. lacunosum–moleculare* and their peak negativity was taken as time = 0 for further analysis. Independently, LFP peaks exceeding 1–3 SD were similarly detected from the CA1 pyramidal cell layer. Negative events in *str. lacunosum–moleculare* with a half-width of 20–65 ms co-occurring with positive peaks in the pyramidal cell layer within ±50 ms time window were considered as putative eSPWs. All pre-detected events were visually inspected (1) to have characteristic waveform with a prominent negative LFP deflection in *str. radiatum*, LFP reversal near the pyramidal cell layer and neuronal firing within the layer, and (2) to discard from analysis in case of coincidence with network oscillatory events.

The eSPW amplitude and half-width were assessed using LFP trace from the recording site located in *str. lacunosum–moleculare*. The CSD analysis was performed on LFP traces normalized to the maximum amplitude signal across all channels and averaged across events. The CSD was calculated for each recording site according to a differential scheme for the second derivative and smoothed with a triangular kernel of length 3. eSPW CSD profiles were built using average current density values averaged within [−5; 5] ms from eSPW peaks. For MUA analysis, raw LFP recordings were band-pass filtered (250–4000 Hz, Daubechies wavelet filter), and action potentials were detected as negative peaks below 4.2 SD of the least active 100 s long epoch over the entire recording.

Only the animals showing well-detectable and stable neuronal firing in the pyramidal cell layer throughout the length of the recording session were considered for MUA analysis. Peri-event time histograms (PETHs) were calculated for MUA in 1 ms bins relative to the eSPW times followed by smoothing with the 10 ms window sliding average filter.

Statistical analysis was performed using the MATLAB Statistics toolbox. Group comparisons were performed using the two-sided Wilcoxon rank sum and Wilcoxon signed rank tests. Unless indicated, group data are presented as median (1st quartile—3rd quartile).

2.5 | Drugs

The glutamate and GABA(A) receptor antagonists CNQX (Tocris Bioscience, UK), D-AP5 (Tocris Bioscience, UK), and 1(S),9(R)-(−)-bicuculline methiodide (Sigma-Aldrich, Switzerland) were applied to the superfused hippocampus with

a perfusing ACSF solution. The ACSF solution was also used to prepare gel from low gelling temperature agarose powder (Sigma-Aldrich, Switzerland).

3 | Results

To test whether the installation of superfusion chamber, which involves removing a section of neocortex, affects the hippocampal network activity we compared electrophysiological properties of eSPWs recorded in the superfused hippocampus preparation and in the hippocampus of neonatal (P5-7) rats with a preserved neocortex. The comparison was performed in two experimental groups. In the first group, eSPW frequency, amplitude, half-width, and multiple unit activity (MUA) were compared between 20 and 60 min-long standard hippocampal recordings from rat pups with intact neocortex and the recordings from the superfused hippocampus of rats with a superfusion chamber installed in one of the cerebral hemispheres. In the second group, eSPW properties were assessed in the left (superfused) and right (intact) hippocampi of the same animal.

When recorded from hippocampi of different animals the eSPW amplitude and half-width in the superfused hippocampus were of 305 (227–463) μV and 55 (49–69) ms ($n = 18$ rats), respectively, and did not differ significantly from the intact hippocampi, where eSPW amplitude reached 413 (314–500) μV ($n = 10$ rats, $p = 0.157$; Figure 1B,C), and the eSPWs half-width was of 47 (41–52) ms ($n = 10$ rats; $p = 0.098$). The frequency of eSPWs attained 1.2 (0.9–1.4) min^{-1} in the superfused hippocampus ($n = 18$) and 1.5 (1.0–1.8) min^{-1} in the intact hippocampus ($n = 10$, $p = 0.221$; Figure 1C). The current-source density (CSD) analysis showed that both CA1 current sinks typical for eSPWs were presented in *str. radiatum* (sink 1) and *str. lacunosum-moleculare* (sink 2) of superfused hippocampus ($n = 18$; Figure 1B). A part of entorhinal cortical projection fibers are known to pass via alveus overlying the dorsal hippocampus (Deller et al. 1996). Obviously, during elimination of the overlying neocortex these fibers are cut, at least partially; therefore the amplitude of the sink 2 of eSPWs recorded in the superfused hippocampus may be affected. Suggesting this, we also assessed the sink1/sink2 ratio to verify that the synaptic activation provided by entorhinal cortex and revealed by sink 2 was preserved in the superfused hippocampus preparation. We found no difference in this ratio between intact and superfused hippocampi, where the ratio values were 0.9 (0.4–1.1) ($n = 10$ rats) and 0.9 (0.5–1.1), respectively ($n = 18$ rats; $p = 0.942$; Figure 1C), hence the superfusion chamber installation did not alter the entorhinal input activation during eSPWs. The comparison of neuronal firing in the CA1 pyramidal layer showed that a baseline MUA in the superfused hippocampus occurred with a frequency of 3.0 (2.2–4.4) s^{-1} ($n = 18$ rats), and MUA frequency in the intact hippocampus was 2.2 (1.2–3.0) s^{-1} ($n = 9$ rats; $p = 0.117$; Figure 1D). The MUA calculated within a time window of [−50; 100] ms from the eSPW peak also here a similar frequency in the superfused and intact hippocampi, which attained 38.4 (16.9–51.5) s^{-1} ($n = 18$ rats) and 24.8 (20.4–32.4) s^{-1} ($n = 9$ rats; $p = 0.425$; Figure 1D), respectively.

Consistent with previous studies (Valeeva, Nasretdinov, et al. 2019; Dard et al. 2022), eSPWs coincided bilaterally in the intact and superfused hippocampi of the same animal with a high probability. When assessed within ±300 ms time window, 91% ± 5% of eSPWs generated in the intact hippocampus co-occurred with eSPWs in the superfused hippocampus, and 90% ± 2% of eSPWs in the superfused hippocampus co-occurred with eSPWs in the contralateral intact hippocampus ($n = 6$ rats). At the same time, eSPWs tended to lead in the intact hippocampus, where the eSPW peak time occurred 11.5 (8.7–14.6) ms ahead of that in the contralateral superfused hippocampus ($n = 6$ rats; $p = 0.063$). The delay of similar length between two hemispheres was also described in neonatal mice carrying a window implant on the hippocampus of one hemisphere with the removed overlying neocortex (Dard et al. 2022) and in the neonatal rats with intact neocortices of both hemispheres, where majority of eSPWs appeared synchronously in the left and right hippocampi, but some eSPWs occurred with ~10 ms time lag (Valeeva, Nasretdinov, et al. 2019). The eSPW half-width was of 57 (54–58) ms and 54 (53–55) ms ($n = 6$ rats; $p = 0.563$) in the intact and superfused hippocampi of one animal, and eSPW amplitude reached 316 (238–435) μV and 372 (196–488) μV, respectively ($n = 6$ rats; $p = 0.563$; Figure 1B,C). The eSPW frequency attained 1.0 (0.8–1.1) min^{-1} in the superfused hippocampus and 0.9 (0.7–1.2) min^{-1} in the contralateral intact hippocampus ($n = 6$, $p = 0.563$; Figure 1C). The sink1/sink2 ratio values were of 1.2 (0.8–2.3) in the intact and 0.8 (0.6–1.1) in the superfused hippocampus ($p = 0.156$, $n = 6$ rats). We did not perform the comparison of neuronal activity in CA1 pyramidal layer of left and right hippocampi as 2 animals had barely detectable baseline and eSPW associated MUA (< 0.5 APs/s) in the intact hippocampus and therefore were excluded from statistical analysis. The MUA values in 4 individual P6-7 rats are shown in Figure 1D. We also checked a possibility that eSPWs were not generated in the superfused hippocampus, but transmitted from the contralateral hemisphere with intact neocortex via commissural fibers. With this aim, we installed two superfused chambers bilaterally at the same coordinates. One chamber was filled with low melting point agarose gel to prevent the hippocampal surface from drying during recording, and hippocampal activity was recorded in the second chamber perfused with ACSF solution. In these recordings, eSPWs still occurred with an amplitude of 352 (237–469) μV, a half-width of 48 (43–48) ms, a frequency of 0.8 (0.6–1.3) min^{-1}, and both current sinks in the *str. radiatum* and *str. lacunosum-moleculare* ($n = 4$ P5-7 rats, data not shown) indicating generation of eSPWs in superfused hippocampus independent of the contralateral hemisphere.

Taken together, the statistical comparisons revealed no differences in eSPW properties and baseline neuronal firing in CA1 pyramidal layer between recordings from superfused hippocampus and hippocampal recordings from rats with the intact neocortex, evidencing for the former to preserve native hippocampal network activity.

We further assessed the effects of selective ionotropic glutamate receptor antagonist application on eSPW parameters. During control recordings, the hippocampal surface was continuously perfused with ACSF solution; subsequently, antagonists were added to the perfusion. To anticipate a drug dilution as it penetrates into the tissue depth, we applied antagonist concentrations 2–3 times exceeding the concentrations used in vitro for complete receptor blockade (Minlebaev

et al. 2007; Vinokurova et al. 2018). The AMPA/kainate receptor antagonist CNQX (40 μM) caused a decrease in eSPW frequency, which dropped to 0.4 (0.3–0.5) min^{-1} after 15–25 min of application compared to 1.3 (0.7–1.7) min^{-1} in control ($n = 8$ rats; $p = 0.008$; Figure 2A,D). In the presence of CNQX, eSPW amplitude decreased to 167 (94–270) μV and eSPW half-width increased to attain 74 (64–96) ms compared to control values of 404 (214–441) μV ($n = 8$ rats; $p = 0.008$) and 59 (53–70) ms, respectively ($n = 8$ rats; $p = 0.008$; Figure 2B,D). The AMPA/kainate receptor blockade also caused a drop in the frequency of neuronal spiking associated with eSPWs in the CA1 pyramidal cell layer (peak MUA frequency was 0.16 (0.09–0.23)

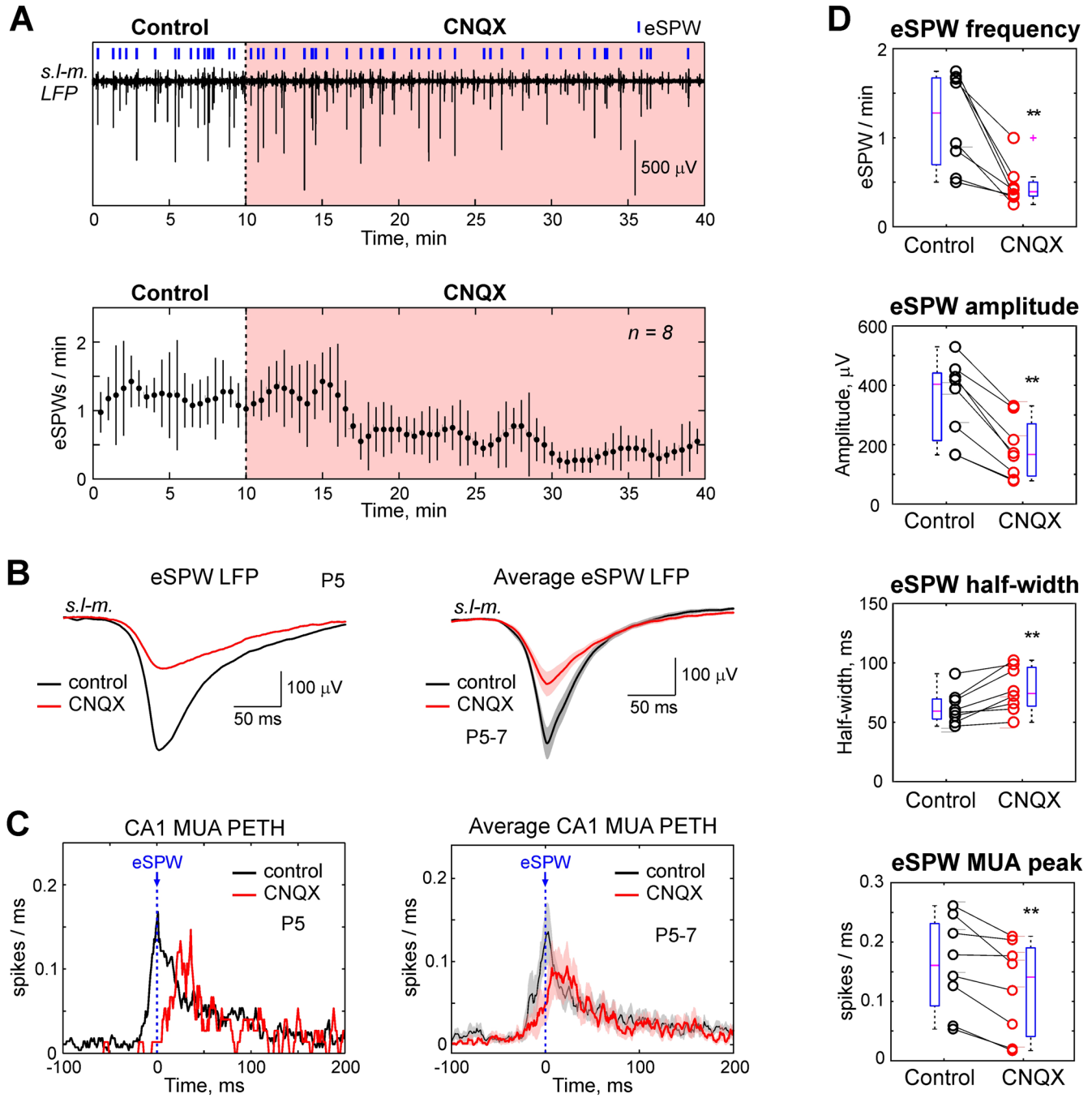

FIGURE 2 | The effect of glutamate AMPA/kainate receptor blockade on eSPW properties. (A) Example trace of local field potential (LFP) recording in str. lacunosum-moleculare (*s.l-m.*) of P7 superfused hippocampus in control and after AMPA/kainate receptor antagonist CNQX (40 μM) application. eSPWs are marked by blue strokes. *Below*, group data (mean ± SE; $n = 8$ P5-7 rats) on the dynamics of eSPW frequency during control and after CNQX application. (B) eSPW LFPs in control and in the presence of CNQX recorded from a P5 rat (*left*) and averaged over 8 P5-7 rats (*right*). (C) Individual P5 rat (*left*) and averaged over 8 P5-7 rats (*right*) PETHs of multiple unit activity (MUA) recorded in CA1 pyramidal cell layer during eSPWs in control and in the presence of CNQX. The curves with shaded areas on panels B and C show mean ± SE. (D) Group data on eSPW amplitude, half-width, frequency and CA1 MUA peak frequency calculated within [−50; 100] ms interval around eSPW LFP peak in control and in the presence of CNQX. Each pair of circles corresponds to an individual rat pup. Boxplots show a median (center line), Q1 and Q3 quartiles (edges), non-outlier extremes (whiskers) and outliers ('+' marker symbols). $^{**}p < 0.01$.

spikes/ms in control and 0.14 (0.03–0.19) spikes/ms in the presence of CNQX; $n = 8$ rats; $p = 0.008$; Figure 2C,D), and shifted the rising side of MUA PETH to the right, indicating a suppression of the fast component of glutamate-mediated excitation ($n = 6$ rats; $p = 0.03$; Figure 2C). We also compared the CNQX effect with the change in eSPW parameters over the same recording period in ACSF to exclude the influence of potential changes in brain state, depth of anesthesia, or recording stability independent of the antagonist effects (Figure 8). The eSPW frequency measured after 40 min of recording in ACSF attained 79 (62–124) % compared to the first 20 min of recording ($p = 0.844$; $n = 6$ rats). The eSPW amplitude and half-widths were 99 (98–110) % ($p = 1.0$; $n = 6$ rats) and 97 (86–108) % ($p = 0.844$; $n = 6$ rats), respectively, and peak MUA frequency attained 98 (78–112) % ($p = 1.0$; $n = 6$ rats) by the end of 1 h-long recording in ACSF. Statistical comparison of these values with the magnitude of CNQX effects also confirmed the suppressive action of the antagonist on eSPW parameters (Figure 8B).

The fact that CNQX suppressed, but did not completely abolish, eSPWs may be due to the limited drug penetration into the deeper hippocampal strata required for eSPW generation. To test this assumption, we assessed the amplitude of the LFP response evoked at different depths of the CA1 hippocampus by electrical stimulation of entorhinal cortex fibers passing within the angular bundle during application of CNQX (Figure 3A,B). The response amplitude was measured

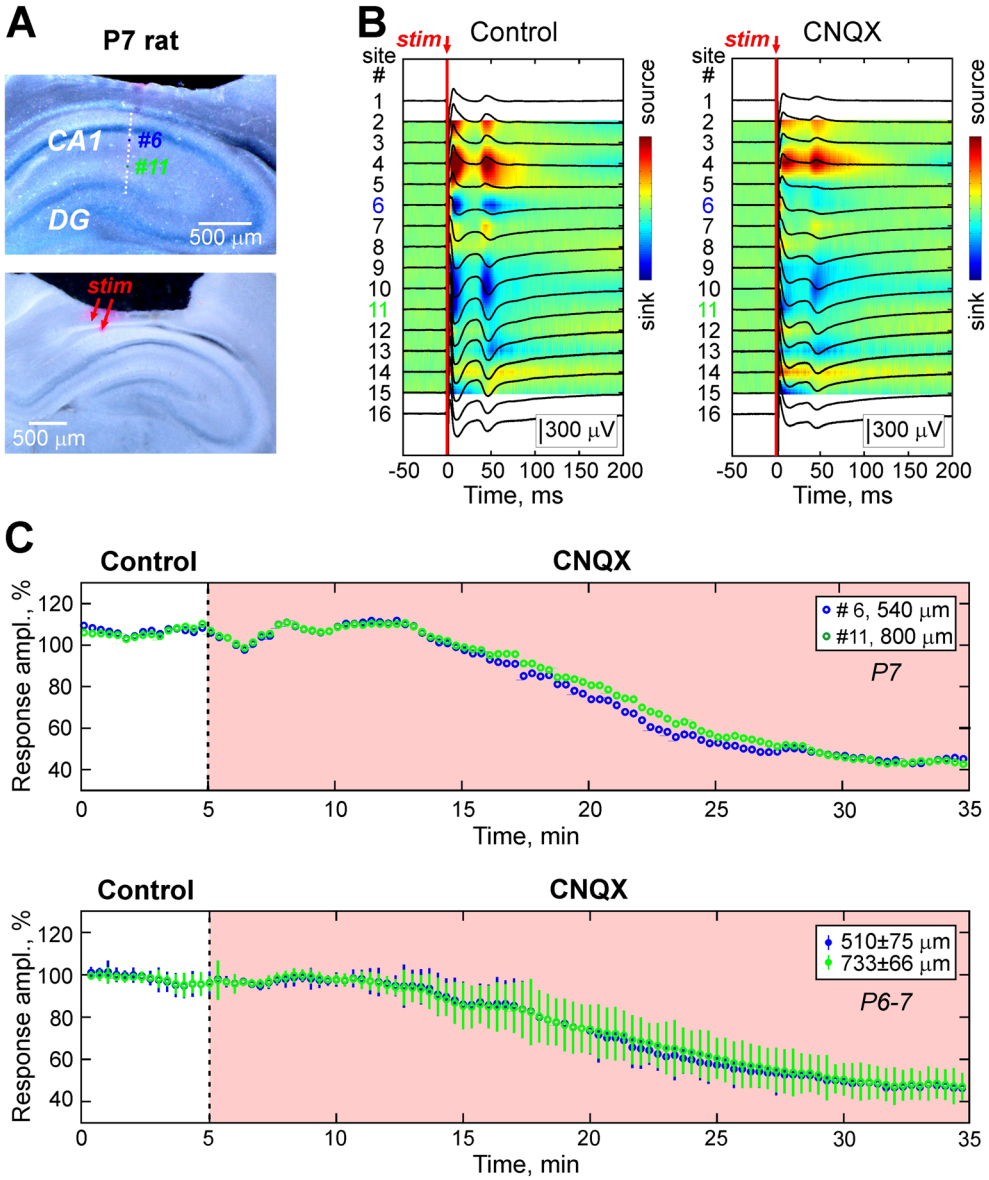

FIGURE 3 | An assessment of CNQX effect on hippocampal response evoked by electrical stimulation of entorhinal cortex fibers at different depths of superfused CA1 hippocampus. (A) The microphotographs of cresyl violet stained hippocampal slices of P7 rat showing the location of the stimulating electrode shanks (marked with red arrows, *top*) and recording sites (*bottom*). (B) Averaged hippocampal LFP responses on electrical stimulation in control (*left*) and in the presence of 40 μM CNQX (*right*) overlaid on current-source density maps. The time of stimulus is indicated with arrows and vertical red lines. (C) The dynamics of changes in the amplitude of hippocampal response recorded at different depths of the CA1 hippocampus in control and during CNQX application. Top graph shows data obtained from individual animal (also presented on panels (A) and (B)), and the bottom graph shows group data (mean ± SE; $n = 4$ P6-7 rats).

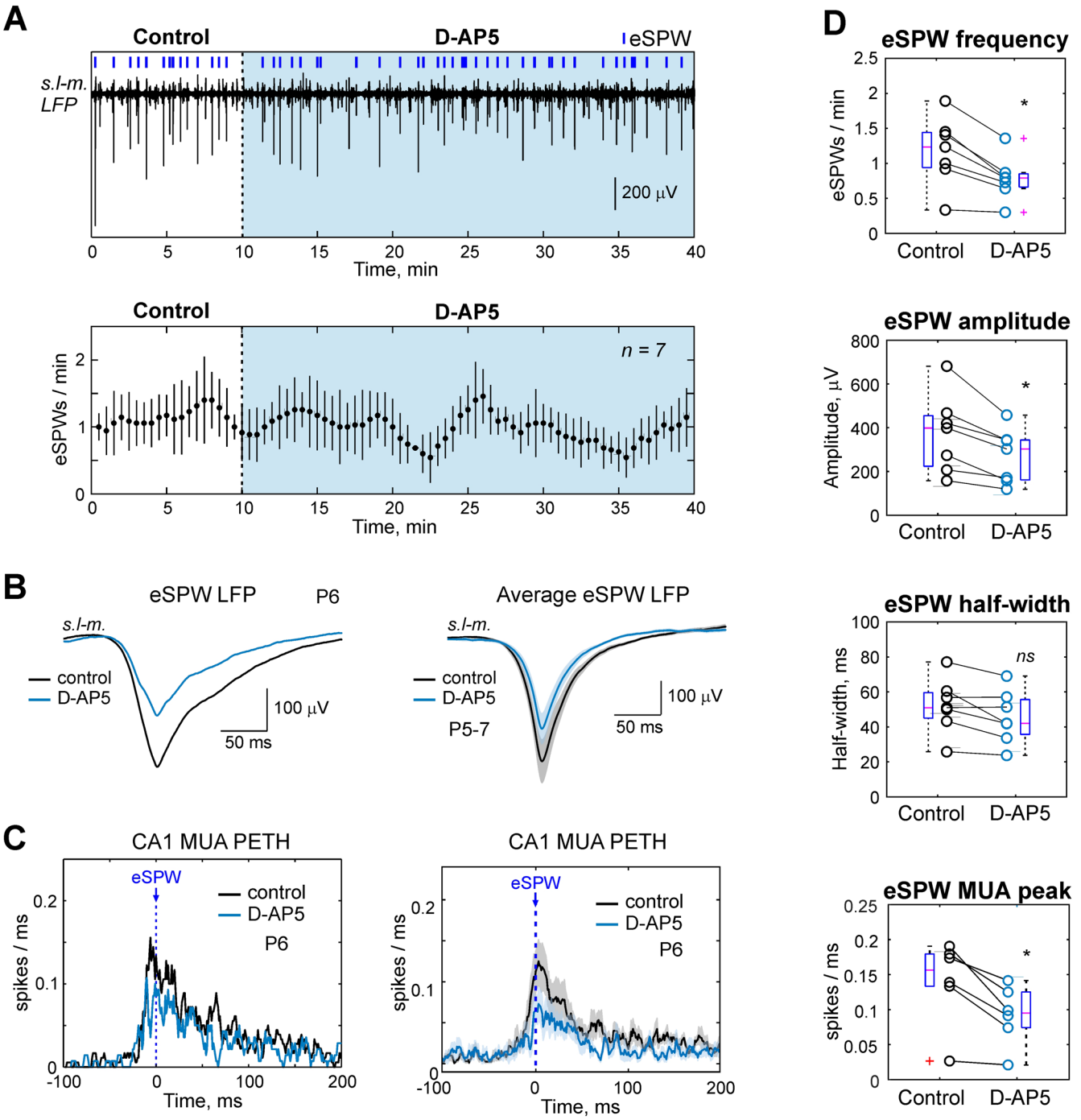

FIGURE 4 | The effect of glutamate NMDA receptor blockade on eSPW properties. (A) Example trace of local field potential (LFP) recording in str. lacunosum-moleculare (*s.l-m.*) of P5 superfused hippocampus in control and after NMDA receptor antagonist D-AP5 (80 μM) application. eSPWs are marked by blue strokes. *Below*, group data (mean ± SE; $n = 7$ P5-7 rats) on the dynamics of eSPW frequency in control and after D-AP5 application. (B) eSPW LFPs in control and in the presence of D-AP5 recorded from P6 rat (*left*) and averaged over 7 P5-7 rats (*right*). (C) Individual P6 rat (*left*) and averaged over 6 P5-7 rats (*right*) PETHs of multiple unit activity (MUA) recorded in CA1 pyramidal cell layer during eSPWs in control and in the presence of D-AP5. The curves with shaded areas on panels B and C show mean ± SE. (D) Group data on eSPW amplitude, half-width, frequency and CA1 MUA peak calculated within [−50; 100] ms interval around eSPW LFP peak in control and in the presence of D-AP5. Each pair of circles corresponds to an individual rat pup. Boxplots show a median (center line), Q1 and Q3 quartiles (edges), non-outlier extremes (whiskers) and outliers ('+' marker symbols). *$p < 0.05$; ns—non-significant.

on recording channels located in the area of the main current sinks in *str. radiatum* (290–640 μm from the surface) and *str. lacunosum-moleculare* (540–840 μm from the surface). In case of gradual drug effect throughout the hippocampal depth, the response amplitude at deeper recording sites was expected to decrease later and to a lesser extent than the amplitude at more superficial sites due to incomplete receptor saturation as it was shown for epipial CNQX application on adult rat neocortex (Vinokurova et al. 2018). However, we observed rather uniform dynamics and degree of response

amplitude suppression in both the superficial and deep hippocampal layers ($n = 4$ P6-7 rats; Figure 3C). At the mean recording depths (which varied depending on the thickness of remaining corpus callosum fibers and the position of current sink) of 510 ± 75 μm and 733 ± 66 μm, LFP response amplitude dropped by 55% ± 4% and 55% ± 7% 20 min after CNQX application, respectively (from 202 (174–217) μV to 83 (78–94) μV at superficial sites ($p < 0.001$), and from 648 (488–793) μV to 251 (222–338) μV at deep sites ($p < 0.001$); $n = 4$ rats; Figure 3C). Thereby, the dynamics of CNQX applied via the superfusion chamber was comparable with in vitro application of the antagonist and completely perfused the hippocampus.

The amplitude of eSPWs was slightly decreased by NMDA receptor antagonist D-AP5 (80 μM) to 303 (162–344) μV compared to 399 (224–455) μV in control ($n = 7$ rats; $p = 0.016$; Figure 4B,D), but no significant D-AP5 effect on eSPW half-width was detected (51 (45–60) ms in control and 42 (36–56) ms in the presence of D-AP5; $n = 7$ rats; $p = 0.078$; Figure 4B,D). The D-AP5 also reduced the eSPW frequency, which decreased from 1.2 (0.9–1.4) min^{-1} in control to 0.8 (0.7–0.8) min^{-1} in the presence of D-AP5 ($n = 7$ rats; $p = 0.031$; Figure 4A,D). Peak MUA frequency was decreased by D-AP5 attaining 0.16 (0.13–0.18) spikes/ms in control recordings and 0.10 (0.07–0.13) spikes/ms in the presence of D-AP5 ($n = 6$ rats, $p = 0.031$; Figure 4C,D). The comparison of D-AP5 effect with a change in eSPW parameters over the same time course in ACSF also showed the decrease in eSPW amplitude and peak MUA frequency, but revealed an insignificant change in the frequency of eSPWs (Figure 8). The latter, therefore, could result from fluctuations in the network state not related to D-AP5 application.

Although blocking either AMPA/kainate or NMDA glutamate receptors separately caused a decrease in eSPW amplitude and frequency, it did not result in eSPW suppression. At the same time, a combined application of both receptor type antagonists completely abolished eSPWs ($n = 6$ rats; $p = 0.008$; Figure 5). The effect was identical whether D-AP5 was added to the perfusion solution containing CNQX, or vice versa: CNQX was applied in the presence of D-AP5.

Next, we assessed an influence of ionotropic and metabotropic GABA receptor blockade on eSPWs. The GABA(A) receptor antagonist bicuculline is known to evoke epileptiform activity both in vitro and in vivo (Baram and Snead 1990; Khalilov et al. 1997; Maier et al. 2003; Isaev et al. 2005; Wu et al. 2005; Ellender et al. 2010). In our experiments, application of 50 μM bicuculline induced high-amplitude epileptiform discharges (Figure 6A,E) alternating with eSPWs, which persisted after GABA(A) receptor blockade, albeit with a reduced frequency. In different animals, 5%–49% of all detected eSPWs were followed by the discharge starting within the next 100 ms. These eSPWs were discarded from analysis of eSPW amplitude and half-widths as their waveform was distorted by epileptiform activity. The eSPWs occurred with a frequency of 1.6 (1.2–2.1) min^{-1} and 1.0 (0.8–1.1) min^{-1} before and after bicuculline application, respectively ($n = 6$ rats, $p = 0.031$; Figure 6A,D). The eSPW amplitude also reduced attaining 416 (289–464) μV in control and 283 (230–328) μV in the presence of bicuculline ($n = 6$ rats, $p = 0.031$; Figure 6A,B,D), while eSPW half-width did not change (53 (43–57) ms in control and 54 (52–66) ms in the presence of bicuculline; $n = 6$ rats; $p = 0.156$; Figure 6B,D). Peak frequency of MUA associated with eSPWs attained 0.11 (0.06–0.14) spikes/ms in control and 0.05 (0.04–0.08) spikes/ms in the presence of bicuculline ($n = 6$ rats, $p = 0.156$; Figure 6C,D), and the bicuculline effect on MUA was also insignificant compared to the change in peak MUA during eSPWs recorded over the same time course in ACSF (Figure 8B). At the same time, eSPW MUA peak time was more delayed relative to eSPW LFP peak in bicuculline compared to control attaining, respectively, 30 (19–36) ms and 1.5 (−5–4) ms ($n = 6$ rats; $p = 0.031$; Figure 6C). It is worth noting that the described effects of GABA(A) receptor blockade on eSPW amplitude and MUA peak time most obviously are

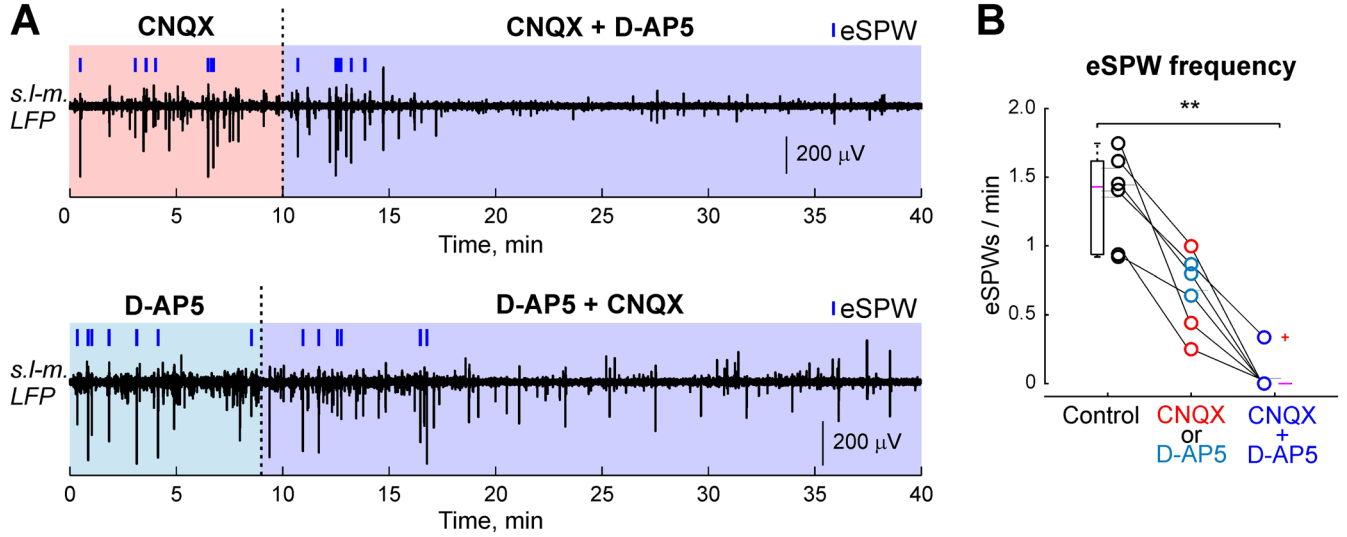

FIGURE 5 | The eSPWs cessation during combined application of AMPA/kainate and NMDA receptor antagonists. (A) Example traces of local field potential (*LFP*) recording in str. lacunosum-moleculare (*s.l-m.*) of superfused hippocampus in the presence of AMPA/kainate receptor antagonist CNQX (P6 rat, upper trace) or NMDA receptor antagonist D-AP5 (P5 rat, lower trace) and during further simultaneous application of CNQX and D-AP5. eSPWs are marked by blue strokes. (B) Group data on eSPWs frequency in control (ACSF), in the presence of CNQX or D-AP5 and after combined application of both antagonists ($n = 6$ P5-7 rats). **$p < 0.01$.

indirect and result from use-dependent depression at glutamatergic synapses developed during high intensity epileptiform activity (see also Discussion section and comparative data presented in Figure 8, which did not confirm the decrease in the frequency of eSPWs after bicuculline application). This primarily concerns CA3—CA1 synapses in *str. radiatum*, which are strongly activated during epileptiform discharges (Figure 6E,F). We found that the amplitude of eSPW sink 1 in *str. radiatum* decreased from 35 (29–45) to 15 (11–17) after the onset of epileptiform activity indicating a reduction in

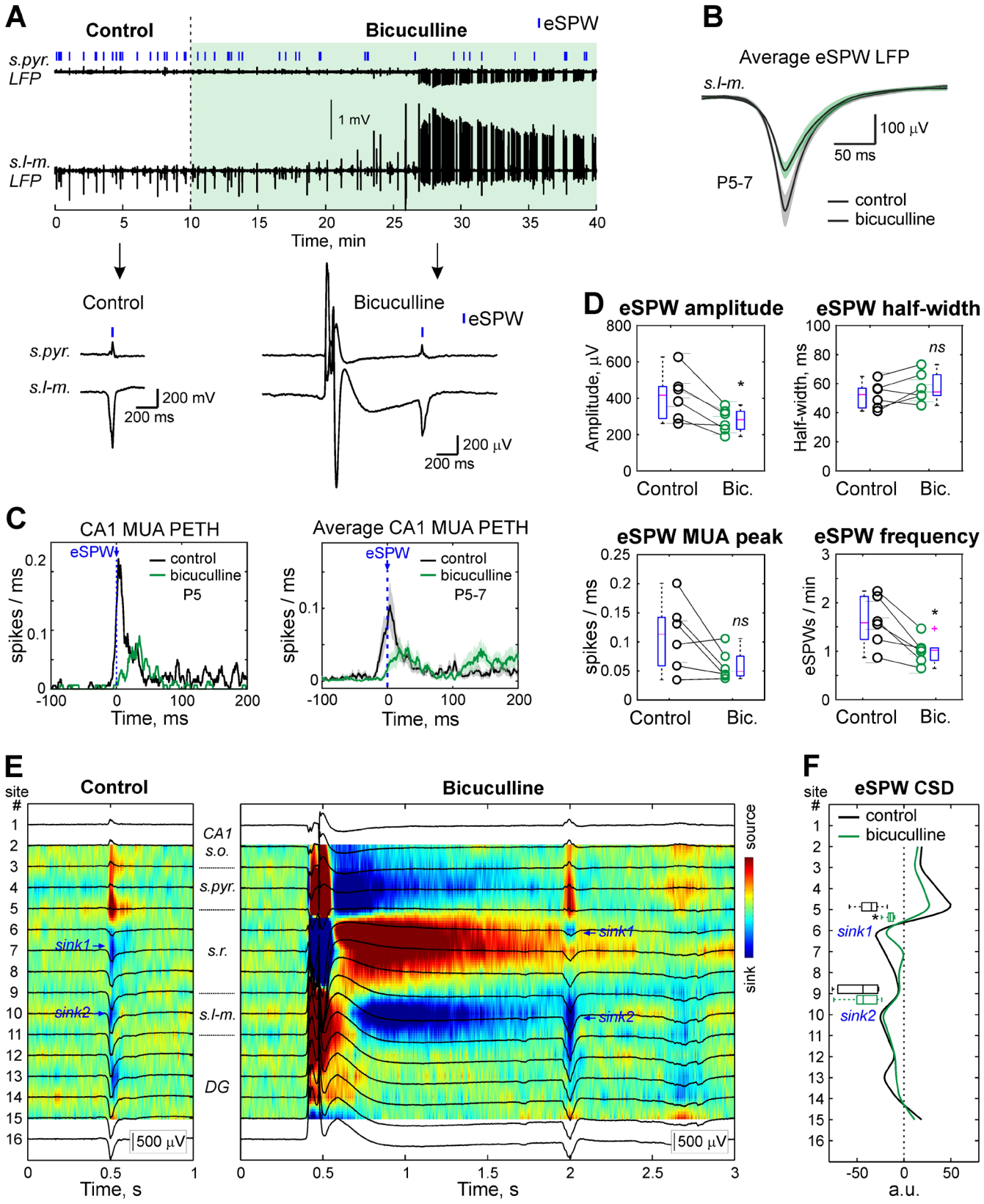

FIGURE 6 | Legend on next page.

FIGURE 6 | The eSPWs persist after GABA(A) receptor blockade. (A) Example traces of local field potential (LFP) recording in str. pyramidale *(s.pyr.)* and str. lacunosum-moleculare (*s.l-m*.) of P7 superfused hippocampus in control and after the application of GABA(A) receptor antagonist bicuculline (50 μM) evoking epileptiform activity. eSPWs are marked by blue strokes. Below the traces, examples of individual eSPW in control (*left*) and eSPW following epileptiform discharge in the presence of bicuculline (*right*) are shown on an expanded timescale. (B) Average eSPW LFPs recorded in CA1 hippocampal *s.l-m*. of 6 P5-7 rats in control and in the presence of bicuculline. (C) Averaged over 6 P5-7 rats PETH of multiple unit activity (MUA) recorded in CA1 pyramidal cell layer during eSPWs in control and in the presence of bicuculline. The curves with shaded areas on panels B and C show mean ± SE. (D) Group data on eSPW amplitude, half-width, frequency and CA1 MUA peak calculated within [−50; 100] ms interval around eSPW LFP peak in control and in the presence of bicuculline. *$p < 0.05$; ns—non-significant. (E) CSD maps of individual eSPW in control and eSPW following epileptiform discharge after bicuculline application. DG—dentate gyrus, *s.o.*—stratum oriens and *s.r.*—stratum radiatum of CA1 hippocampus. (F) CSD profiles at the peak of eSPWs from the recording presented on panels A and D. Boxplots show group data on the amplitude of CA1 current sinks during eSPWs.

excitatory input from CA3 to CA1 pyramidal layer neurons ($n = 6$ rats; $p = 0.031$), whereas sink 2 amplitude representing synaptic input from entorhinal cortex layer 3 did not change (Figure 6F). The reduction of glutamate release at CA3—CA1 synapses might also cause the desynchronization of AP generation in CA1 pyramidal layer and the shift of eSPW MUA PETH peak toward more delayed values, similar to the delayed AP generation in response to subthreshold EPSPs (Fricker and Miles 2000) at hippocampal glutamatergic synapses and to the slowdown of excitation dynamics at neonatal GABAergic synapses in vitro (Valeeva et al. 2010). As one of the synaptic inputs (sink 1) contributing to LFP during eSPWs was reduced we also observed a decrease in eSPW amplitude despite another input (sink 2) remaining unchanged.

In contrast to bicuculline, the application of metabotropic GABA(B) receptor antagonist CGP55845 (2 μM) did not evoke epileptiform activity. The eSPW properties were not affected by the antagonist as well. In control recordings, eSPW frequency was 0.6 (0.5–1.1) min^{-1} and did not change 20 min after CGP55845 application attaining 0.7 (0.6–1.0) min^{-1} ($n = 6$ P5-6 rats; $p = 0.563$; Figure 7A,D). The eSPW amplitude was 300 (246–337) and 254 (210–276) μV ($n = 6$ P5-6 rats; $p = 0.063$; Figure 7B,D) and eSPW half-width was 62 (59–71) and 62 (54–70) ms ($n = 6$ P5-6 rats; $p = 0.688$; Figure 7B,D) in control and in the presence of CGP55845 respectively. Peak MUA frequency attained 0.09 (0.03–0.15) spikes/ms during eSPWs in control and 0.10 (0.06–0.14) after CGP55845 application ($n = 6$ P5-6 rats; $p = 0.438$; Figure 7C,D). These results (as well as data presented in Figure 8) reveal that GABA(B) receptor activation does not contribute to eSPWs in the neonatal hippocampus.

4 | Discussion

To explore the impact of different subtypes of glutamate and GABA receptor blockade on electrophysiological properties of eSPWs in neonatal rat hippocampus in vivo we have employed a superfused hippocampus technique. This technique allows a direct and continuous application of pharmacological substances to the large area of the hippocampal surface. Comparing the properties of eSPWs recorded from superfused hippocampus and acquired during conventional in vivo recordings, we have shown that eSPWs do not differ between two recording conditions, and the superfused hippocampus technique is suitable for investigation of rat hippocampal activity as early as the first week of neonatal development. Using selective receptor antagonists, we have also demonstrated that both ionotropic glutamate receptor subtypes are involved in the generation of eSPWs, whereas the participation of GABA receptors does not seem to be crucial.

According to in vitro studies, the AMPA/kainate glutamate receptor blockade eliminates GDPs in neonatal hippocampus (Ben-Ari et al. 1989; Bolea et al. 1999), and completely suppresses or reduces SPW-Rs in adult hippocampal slices (Papatheodoropoulos and Kostopoulos 2002; Maier et al. 2003; Wu et al. 2005; Ellender et al. 2010; Hofer et al. 2015). In our experiments, blocking the AMPA/kainate receptors also produced a depressing effect on eSPW frequency and amplitude; however, it did not cause complete eSPW suppression unless applied together with NMDA receptor antagonist D-AP5. The latter reveals an additive effect of two glutamate receptor subtype activation and an important contribution of NMDA receptors to eSPW generation. In this regard, eSPWs should obviously facilitate the NMDA dependent synaptic plasticity supporting network formation in the developing hippocampus (Isaac et al. 1995; Durand et al. 1996; Voronin and Cherubini 2004; Hu et al. 2019). The inhibition of eSPWs caused by combined action of two glutamate receptor antagonists was similar to the effect produced by presynaptic chemogenetic silencing of glutamatergic neurotransmission in neonatal hippocampus in vivo (Graf et al. 2024). The blocking of NMDA receptors alone also reduced eSPW frequency and amplitude, just as it was described for D-AP5 effect on GDP frequency (Bolea et al. 1999). At the same time, NMDA receptor activation is not obligatory for SPW-R generation. Most studies report that NMDA receptor blockade has no effect on electrophysiological properties of SPW-Rs (Bolea et al. 1999; Maier et al. 2003; Behrens et al. 2005; Hofer et al. 2015). When detected, this effect is limited to eSPW-R amplitude modulation (Colgin et al. 2005; Ellender et al. 2010) or to eSPW-Rs integration into clusters of double or triple events (Papatheodoropoulos 2010).

Pharmacological blockade of GABA(A) receptors causes a transition of GDPs (in neonatal hippocampal slices) and SPW-Rs (in adult animals in vitro) into large epileptiform discharges, and both activity patterns are no longer observed after the onset of paroxysmal activity (Khalilov et al. 1997; Lamsa et al. 2000; Maier et al. 2003; Behrens et al. 2007; Ellender et al. 2010; Valeeva et al. 2010). In our experiments, blocking the GABA(A) receptors by bicuculline similarly evoked recurrent epileptiform activity bursts, however eSPW generation also continued in the presence of bicuculline. The resistance

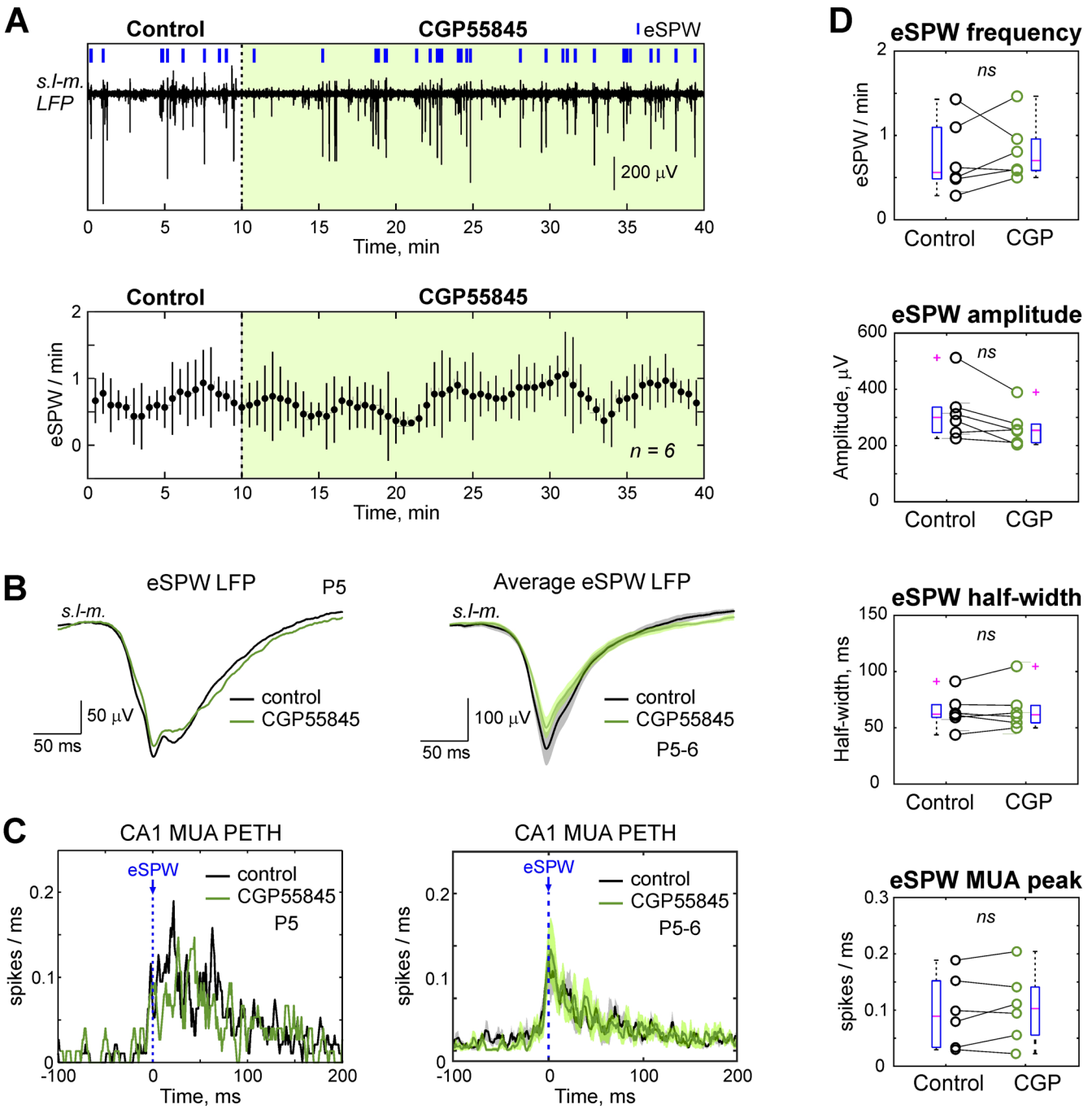

FIGURE 7 | GABA(B) receptor blockade does not affect eSPW properties. (A) Example trace of local field potential (LFP) recording in str. lacunosum-moleculare (*s.l-m.*) of P6 superfused hippocampus in control and after GABA(B) receptor antagonist CGP55845 (2 μM) application. ESPWs are marked by blue strokes. *Below*, group data (mean ± SE; $n = 6$ P5-6 rats) on the dynamics of eSPW frequency in control and after CGP55845 application. (B) eSPW LFPs in control and in the presence of CGP55845 recorded from a P5 rat (*left*) and averaged over 6 P5-6 rats (*right*). (C) Individual P5 rat (*left*) and averaged over 6 P5-6 rats (*right*) PETHs of multiple unit activity (MUA) recorded in CA1 pyramidal cell layer during eSPWs in control and in the presence of CGP55845. The curves with shaded areas on panels B and C show mean ± SE. (D) Group data on eSPW amplitude, half-width, frequency and CA1 MUA peak calculated within [−50; 100] ms interval around eSPW LFP peak in control and in the presence of CGP55845. ns—non-significant.

of eSPWs to GABA receptor blockade reveals a minor role of GABA(A) conductance in eSPW generation or at least in their initiation as GABA(A) receptor mediated currents are activated during eSPWs (Leinekugel et al. 2002). This independence of eSPW generation from GABA(A) receptor involvement well correlates with an absence of functional somatic inhibition in pyramidal cell layer during the first postnatal week (Dard et al. 2022), which coincides in time with a period of eSPW activity pattern expression. Our data are also consistent with the observations made on P7 mice, where neither enhancing, nor suppressing interneuron excitability produced a significant effect on the amplitude, half-widths or frequency of eSPW

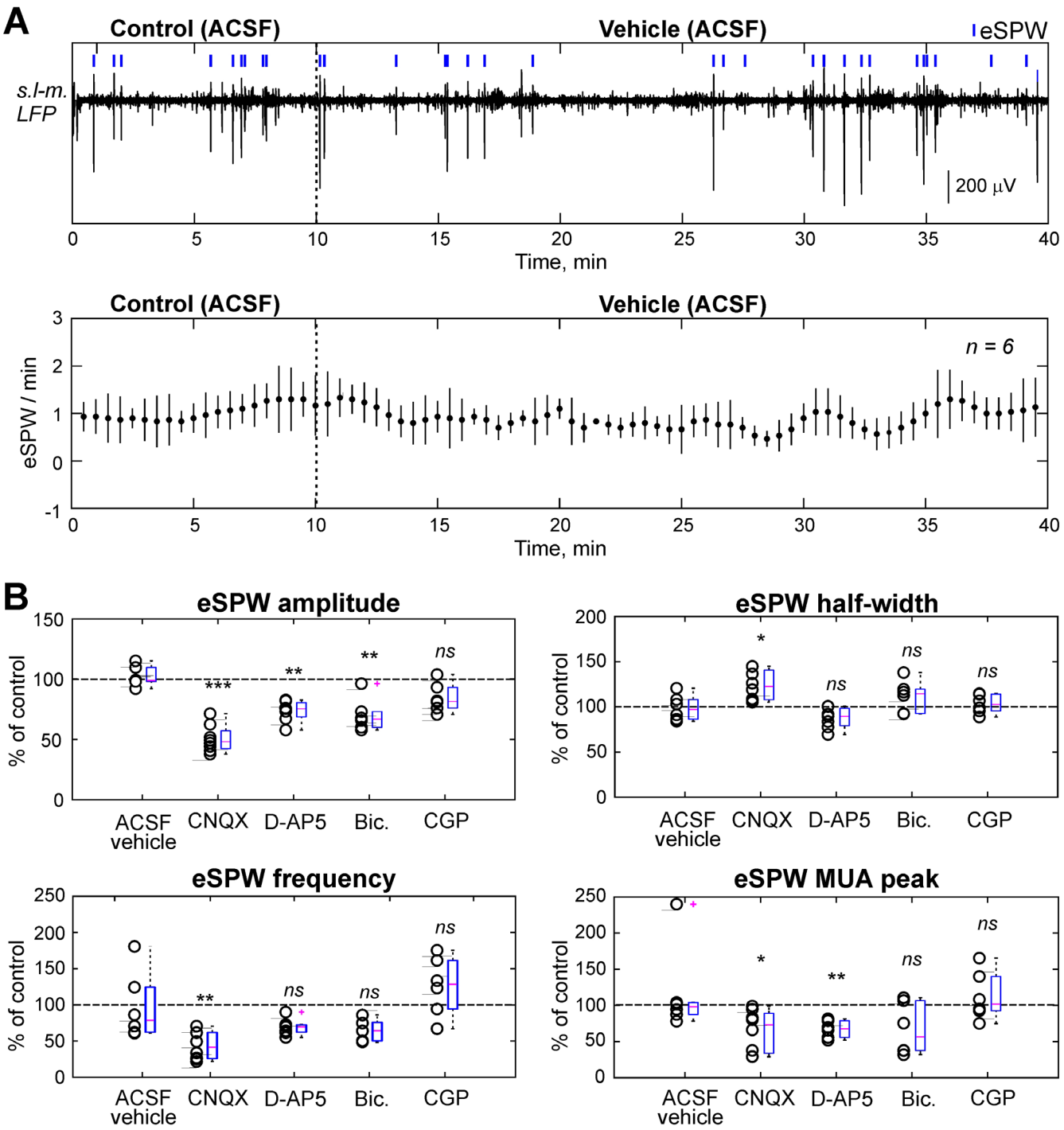

FIGURE 8 | Statistical comparisons between eSPW properties assessed following 40 min of recording in ACSF and in the presence of glutamate and GABA receptor antagonists. (A) Example trace of local field potential (LFP) recording in str. lacunosum-moleculare (*s.l-m.*) of P5 superfused hippocampus in ACSF. ESPWs are marked by blue strokes. *Below*, group data (mean ± SE; $n = 6$ P5-7 rats) on the dynamics of eSPW frequency during 40 min of recording in ACSF. The same time interval from the start of recording is shown as in Figures 2, 4 and 7. (B) Group data on eSPW amplitude, half-width, frequency and eSPW associated peak MUA calculated following 40 min of recording in ACSF and in the presence of CNQX, D-AP5, bicuculline (Bic.) and CGP55845 (CGP).

occurrence (Murata and Colonnese 2020). At the same time, an assessment of effects produced by GABA(A) receptor blockade on eSPW properties is complicated by the emergence of epileptiform activity, which affects the functioning of entire hippocampal network, particularly CA3—CA1 synapses massively activated during epileptiform discharges. Under these conditions, a direct interpretation of the effects of GABA(A) receptor blockade on eSPW properties may lead to a misreading. In this regard, the decrease in eSPW associated MUA frequency in the presence of bicuculline, which could be explained as a decrease in neuronal excitability, obviously results from the suppression of glutamate release from Shaffer collaterals due to their hyperactivation. This synaptic suppression can be seen on the eSPW CSD profile as a reduction of current sink in

str. radiatum. In addition, overall MUA frequency calculated throughout the entire trace including epileptiform discharges shows an increase in neuronal firing from (2.4 (2.0–2.9)) s^{-1} in control to 6.5 (5.6–7.2) s^{-1} in the presence of bicuculline ($n = 6$ rats; $p = 0.031$). Similarly, when the network operation mode is affected by ongoing epileptiform activity, eSPW amplitude and frequency changes, observed in our experiments, are not an appropriate readout to conclude on the modulatory effect of GABAergic transmission on eSPW generation.

The GABA(B) receptors are known to be involved in the termination of GDPs via afterhyperpolarization by activation of potassium channels and presynaptic effects; therefore, the receptor blockade increases the half-widths of GDPs transforming them to interictal- and ictal-like discharges (McLean et al. 1996; Khalilov et al. 2017). The active ripple-following hyperpolarization is also considered as a mechanism of SPW-R termination (Wu et al. 2005; English et al. 2014), however, GABA(B) receptor blockade was not shown to cause epileptiform activity in vitro in rats older than two postnatal weeks (Ellender et al. 2010; Hollnagel et al. 2014; Hofer et al. 2015). The application of GABA(B) receptor antagonists increased the SPW-R incidence in hippocampal slices of adolescent rats (Ellender et al. 2010) and did not affect the amplitude and frequency of SPW-Rs in adult rats in vitro (Hollnagel et al. 2014; Hofer et al. 2015). The latter is similar to our observations on eSPWs that were not affected by GABA(B) receptor blockade, implying that this receptor subtype is not required for eSPW generation, and further supporting a difference in the generative mechanisms of GDPs in vitro and eSPWs in vivo (Juzekaeva et al. 2024). The ictogenic effect produced by GABA(B) receptor antagonists in neonatal hippocampal slices, unlike the slices of adult hippocampus and the neonatal superfused hippocampus, most likely results from limited sources of inhibition as the activation of GABA(A) conductance excites immature neurons in vitro (Ben-Ari et al. 1997; Leinekugel et al. 1997; Pfeffer et al. 2009; Valeeva et al. 2010). At the same time, in adult hippocampal slices and in neonatal hippocampus in vivo, GABA(A) receptors mediate inhibitory effect on the network level (Kirmse et al. 2015; Valeeva et al. 2016; Mortet et al. 2025; but see Murata and Colonnese 2020) that prevents neuronal overexcitation once GABA(B) receptors are blocked.

In the future, it would also be interesting to assess the contribution of electrical synapses to eSPW activity using blockers of gap junctions known to be abundant during early brain development and to be involved in correlated neocortical and hippocampal activity patterns in vitro such as correlated calcium waves, neuronal domains, spontaneous plateau assemblies, GDPs and carbachol-induced beta oscillations (Yuste et al. 1992; Strata et al. 1997; Peinado 2001; Dupont et al. 2006; Crepel et al. 2007). In the neocortex, gap junction blockers were previously shown to have no significant effect on early in vivo activity (Minlebaev et al. 2007; Valiullina et al. 2016), however, experimental data on the effect of electrical coupling blockade on eSPW generation in the hippocampus are lacking.

In summary, we have shown that the superfused hippocampus preparation, which combines the advantages of in vivo recordings and in vitro approaches, is suitable for early hippocampal activity investigation. Using this technique, we have described a receptor mechanism of eSPW generation, which includes predominant glutamatergic receptor engagement and emphasizes the significance of NMDA receptors for early neuronal activity in the developing hippocampus. The superfused hippocampus technique provides additional opportunities for exploring the neurophysiology of the hippocampus during early postnatal development when it is generally difficult to achieve rapid and sufficient expression of a specific gene using standard viral vectors, and applying optogenetic or chemogenetic approaches may also be challenging. It may also facilitate in vivo patch-clamp recordings from the hippocampus, allowing differentiation between interneurons and principal cells, which is a significant limitation of cluster analysis of extracellular spikes recorded from immature neurons due to their lower amplitude and firing rate (Weir et al. 2015; Valeeva, Janackova, et al. 2019).

Acknowledgments

We thank Dr. Roustem Khazipov for providing valuable feedback on the manuscript and research project, as well as Dr. Azat Nasretdinov for helpful suggestions on data analysis.

Ethics Statement

Animal care and procedures were in accordance with EU Directive 2010/63/EU for animal experiments, and all animal-use protocols were approved by the Local Ethical Committee of Kazan Federal University (No 24/22.09.2020).

Conflicts of Interest

The authors declare no conflicts of interest.

Data Availability Statement

The data that support the findings of this study are available from the corresponding author upon reasonable request.

References

Baram, T. Z., and O. C. Snead. 1990. "Bicuculline Induced Seizures in Infant Rats: Ontogeny of Behavioral and Electrocortical Phenomena." *Developmental Brain Research* 57: 291–295. https://doi.org/10.1016/0165-3806(90)90055-4.

Behrens, C. J., L. P. van den Boom, L. de Hoz, A. Friedman, and U. Heinemann. 2005. "Induction of Sharp Wave–Ripple Complexes in Vitro and Reorganization of Hippocampal Networks." *Nature Neuroscience* 8: 1560–1567. https://doi.org/10.1038/nn1571.

Behrens, C. J., L. P. Van Den Boom, and U. Heinemann. 2007. "Effects of the GABA A Receptor Antagonists Bicuculline and Gabazine on Stimulus-Induced Sharp Wave-Ripple Complexes in Adult Rat Hippocampus in Vitro." *European Journal of Neuroscience* 25: 2170–2181. https://doi.org/10.1111/j.1460-9568.2007.05462.x.

Ben-Ari, Y., E. Cherubini, R. Corradetti, and J. L. Gaiarsa. 1989. "Giant Synaptic Potentials in Immature Rat CA3 Hippocampal Neurones." *Journal of Physiology* 416: 303–325. https://doi.org/10.1113/jphysiol.1989.sp017762.

Ben-Ari, Y., R. Khazipov, X. Leinekugel, O. Caillard, and J. L. Gaiarsa. 1997. "GABA(A), NMDA and AMPA Receptors: A Developmentally Regulated "Menage a Trois"." *Trends in Neurosciences* 20: 523–529. https://doi.org/10.1016/S0166-2236(97)01147-8.

Bolea, S., E. Avignone, N. Berretta, J. V. Sanchez-Andres, and E. Cherubini. 1999. "Glutamate Controls the Induction of GABA-Mediated Giant Depolarizing Potentials Through AMPA Receptors in Neonatal

Rat Hippocampal Slices." *Journal of Neurophysiology* 81: 2095–2102. https://doi.org/10.1152/jn.1999.81.5.2095.

Buhl, D. L., and G. Buzsáki. 2005. "Developmental Emergence of Hippocampal Fast-Field "Ripple" Oscillations in the Behaving Rat Pups." *Neuroscience* 134: 1423–1430. https://doi.org/10.1016/j.neuroscience.2005.05.030.

Buzsáki, G. 2015. "Hippocampal Sharp Wave-Ripple: A Cognitive Biomarker for Episodic Memory and Planning." *Hippocampus* 25: 1073–1188. https://doi.org/10.1002/hipo.22488.

Buzsáki, G., L. Lai-Wo, and C. H. Vanderwolf. 1983. "Cellular Bases of Hippocampal EEG in the Behaving Rat." *Brain Research Reviews* 6: 139–171. https://doi.org/10.1016/0165-0173(83)90037-1.

Colgin, L. L., Y. Jia, J.-M. Sabatier, and G. Lynch. 2005. "Blockade of NMDA Receptors Enhances Spontaneous Sharp Waves in Rat Hippocampal Slices." *Neuroscience Letters* 385: 46–51. https://doi.org/10.1016/j.neulet.2005.05.005.

Cossart, R., and R. Khazipov. 2022. "How Development Sculpts Hippocampal Circuits and Function." *Physiological Reviews* 102: 343–378. https://doi.org/10.1152/physrev.00044.2020.

Crepel, V., D. Aronov, I. Jorquera, A. Represa, Y. Ben-Ari, and R. Cossart. 2007. "A Parturition-Associated Nonsynaptic Coherent Activitypattern in the Developing Hippocampus." *Neuron* 54: 105–120. https://doi.org/10.1016/j.neuron.2007.03.007.

Csicsvari, J., H. Hirase, A. Mamiya, and G. Buzsáki. 2000. "Ensemble Patterns of Hippocampal CA3-CA1 Neurons During Sharp Wave–Associated Population Events." *Neuron* 28: 585–594. https://doi.org/10.1016/S0896-6273(00)00135-5.

Dard, R. F., E. Leprince, J. Denis, et al. 2022. "The Rapid Developmental Rise of Somatic Inhibition Disengages Hippocampal Dynamics From Self-Motion." *eLife* 11: e78116. https://doi.org/10.7554/eLife.78116.

Deller, T., G. Adelmann, R. Nitsch, and M. Frotscher. 1996. "The Alvear Pathway of the Rat Hippocampus." *Cell and Tissue Research* 286: 293–303. https://doi.org/10.1007/s004410050699.

Dupont, E., I. L. Hanganu, W. Kilb, S. Hirsch, and H. J. Luhmann. 2006. "Rapid Developmental Switch in the Mechanisms Driving Early Cortical Columnarnetworks." *Nature* 439: 79–83. https://doi.org/10.1038/nature04264.

Durand, G. M., Y. Kovalchuk, and A. Konnerth. 1996. "Long-Term Potentiation and Functional Synapse Induction in Developing Hippocampus." *Nature* 381: 71–75. https://doi.org/10.1038/381071a0.

Ellender, T. J., W. Nissen, L. L. Colgin, E. O. Mann, and O. Paulsen. 2010. "Priming of Hippocampal Population Bursts by Individual Perisomatic-Targeting Interneurons." *Journal of Neuroscience* 30: 5979–5991. https://doi.org/10.1523/JNEUROSCI.3962-09.2010.

English, D. F., A. Peyrache, E. Stark, et al. 2014. "Excitation and Inhibition Compete to Control Spiking During Hippocampal Ripples: Intracellular Study in Behaving Mice." *Journal of Neuroscience* 34: 16509–16517. https://doi.org/10.1523/JNEUROSCI.2600-14.2014.

Fricker, D., and R. Miles. 2000. "EPSP Amplification and the Precision of Spike Timing in Hippocampal Neurons." *Neuron* 28: 559–569. https://doi.org/10.1016/S0896-6273(00)00133-1.

Graf, J., A. Samiee, T. Flossmann, K. Holthoff, and K. Kirmse. 2024. "Chemogenetic Silencing Reveals Presynaptic Gi/o Protein-Mediated Inhibition of Developing Hippocampal Synchrony in Vivo." *iScience* 27: 110997. https://doi.org/10.1016/j.isci.2024.110997.

Graf, J., C. Zhang, S. L. Marguet, et al. 2021. "A Limited Role of NKCC1 in Telencephalic Glutamatergic Neurons for Developing Hippocampal Network Dynamics and Behavior." *Proceedings of the National Academy of Sciences* 118: e2014784118. https://doi.org/10.1073/pnas.2014784118.

Griguoli, M., and E. Cherubini. 2017. "Early Correlated Network Activity in the Hippocampus: Its Putative Role in Shaping Neuronal Circuits." *Frontiers in Cellular Neuroscience* 11: 255. https://doi.org/10.3389/fncel.2017.00255.

Hajos, N., M. R. Karlocai, B. Nemeth, et al. 2013. "Input-Output Features of Anatomically Identified CA3 Neurons During Hippocampal Sharp Wave/Ripple Oscillation in Vitro." *Journal of Neuroscience* 33: 11677–11691. https://doi.org/10.1523/JNEUROSCI.5729-12.2013.

Hofer, K. T., Á. Kandrács, I. Ulbert, et al. 2015. "The Hippocampal CA3 Region Can Generate Two Distinct Types of Sharp Wave-Ripple Complexes, in Vitro." *Hippocampus* 25: 169–186. https://doi.org/10.1002/hipo.22361.

Hollnagel, J. O., A. Maslarova, R. u. Haq, and U. Heinemann. 2014. "GABAB Receptor Dependent Modulation of Sharp Wave-Ripple Complexes in the Rat Hippocampus in Vitro." *Neuroscience Letters* 574: 15–20. https://doi.org/10.1016/j.neulet.2014.04.045.

Hu, H. Y., D. L. H. Kruijssen, C. P. Frias, B. Rózsa, C. C. Hoogenraad, and C. J. Wierenga. 2019. "Endocannabinoid Signaling Mediates Local Dendritic Coordination Between Excitatory and Inhibitory Synapses." *Cell Reports* 27: 666–675.e5. https://doi.org/10.1016/j.celrep.2019.03.078.

Isaac, J. T. R., R. A. Nicoll, and R. C. Malenka. 1995. "Evidence for Silent Synapses: Implications for the Expression of LTP." *Neuron* 15: 427–434. https://doi.org/10.1016/0896-6273(95)90046-2.

Isaev, D., E. Isaeva, R. Khazipov, and G. L. Holmes. 2005. "Anticonvulsant Action of GABA in the High Potassium–Low Magnesium Model of Ictogenesis in the Neonatal Rat Hippocampus in Vivo and in Vitro." *Journal of Neurophysiology* 94: 2987–2992. https://doi.org/10.1152/jn.00138.2005.

Juzekaeva, E., A. Nasretdinov, M. Mukhtarov, D. Shipkov, G. Valeeva, and R. Khazipov. 2024. "Comparison of Extracellular Giant Depolarizing Potentials in Vitro and Early Sharp Waves in Vivo in the CA1 Hippocampus of Neonatal Rats." *Biochemical and Biophysical Research Communications* 735: 150823. https://doi.org/10.1016/j.bbrc.2024.150823.

Karlsson, K. Æ., E. J. Mohns, G. V. di Prisco, and M. S. Blumberg. 2006. "On the Co-Occurrence of Startles and Hippocampal Sharp Waves in Newborn Rats." *Hippocampus* 16: 959–965. https://doi.org/10.1002/hipo.20224.

Katz, L. C., and C. J. Shatz. 1996. "Synaptic Activity and the Construction of Cortical Circuits." *Science* 274: 1133–1138. https://doi.org/10.1126/science.274.5290.1133.

Khalilov, I., R. Khazipov, M. Esclapez, and Y. Ben-Ari. 1997. "Bicuculline Induces Ictal Seizures in the Intact Hippocampus Recorded in Vitro." *European Journal of Pharmacology* 319: R5–R6. https://doi.org/10.1016/S0014-2999(96)00964-8.

Khalilov, I., M. Minlebaev, M. Mukhtarov, E. Juzekaeva, and R. Khazipov. 2017. "Postsynaptic GABA(B) Receptors Contribute to the Termination of Giant Depolarizing Potentials in CA3 Neonatal Rat Hippocampus." *Frontiers in Cellular Neuroscience* 11: 179. https://doi.org/10.3389/fncel.2017.00179.

Khazipov, R., and G. L. Holmes. 2003. "Synchronization of Kainate-Induced Epileptic Activity via GABAergic Inhibition in the Superfused Rat Hippocampus in Vivo." *Journal of Neuroscience* 23: 5337–5341. https://doi.org/10.1523/jneurosci.23-12-05337.2003.

Khazipov, R., X. Leinekugel, I. Khalilov, J. L. Gaiarsa, and Y. Ben-Ari. 1997. "Synchronization of GABAergic Interneuronal Network in CA3 Subfield of Neonatal Rat Hippocampal Slices." *Journal of Physiology* 498: 763–772. https://doi.org/10.1113/jphysiol.1997.sp021900.

Khazipov, R., D. Zaynutdinova, E. Ogievetsky, et al. 2015. "Atlas of the Postnatal Rat Brain in Stereotaxic Coordinates." *Frontiers in Neuroanatomy* 9: 161. https://doi.org/10.3389/fnana.2015.00161.

Kirmse, K., M. Kummer, Y. Kovalchuk, O. W. Witte, O. Garaschuk, and K. Holthoff. 2015. "GABA Depolarizes Immature Neurons and

Inhibits Network Activity in the Neonatal Neocortex in Vivo." *Nature Communications* 6: 7750. https://doi.org/10.1038/ncomms8750.

Lamsa, K., J. M. Palva, E. Ruusuvuori, K. Kaila, and T. Taira. 2000. "Synaptic GABA A Activation Inhibits AMPA-Kainate Receptor–Mediated Bursting in the Newborn (P0–P2) Rat Hippocampus." *Journal of Neurophysiology* 83: 359–366. https://doi.org/10.1152/jn.2000.83.1.359.

Leinekugel, X., R. Khazipov, R. Cannon, H. Hirase, Y. Ben-Ari, and G. Buzsáki. 2002. "Correlated Bursts of Activity in the Neonatal Hippocampus in Vivo." *Science* 296: 2049–2052. https://doi.org/10.1126/science.1071111.

Leinekugel, X., I. Medina, I. Khalilov, Y. Ben-Ari, and R. Khazipov. 1997. "Ca2+ Oscillations Mediated by the Synergistic Excitatory Actions of GABAA and NMDA Receptors in the Neonatal Hippocampus." *Neuron* 18: 243–255. https://doi.org/10.1016/S0896-6273(00)80265-2.

Maier, N., V. Nimmrich, and A. Draguhn. 2003. "Cellular and Network Mechanisms Underlying Spontaneous Sharp Wave–Ripple Complexes in Mouse Hippocampal Slices." *Journal of Physiology* 550: 873–887. https://doi.org/10.1113/jphysiol.2003.044602.

McLean, H. A., O. Caillard, R. Khazipov, Y. Ben-Ari, and J. L. Gaiarsa. 1996. "Spontaneous Release of GABA Activates GABAB Receptors and Controls Network Activity in the Neonatal Rat Hippocampus." *Journal of Neurophysiology* 76: 1036–1046. https://doi.org/10.1152/jn.1996.76.2.1036.

Minlebaev, M., Y. Ben-Ari, and R. Khazipov. 2007. "Network Mechanismsof Spindle-Burst Oscillations in the Neonatal Rat Barrel Cortex in Vivo." *Journal of Neurophysiology* 97: 692–700. https://doi.org/10.1152/jn.00759.2006.

Mohns, E. J., K. Æ. Karlsson, and M. S. Blumberg. 2007. "Developmental Emergence of Transient and Persistent Hippocampal Events and Oscillations and Their Association With Infant Seizure Susceptibility." *European Journal of Neuroscience* 26: 2719–2730. https://doi.org/10.1111/j.1460-9568.2007.05928.x.

Mortet, S., R. Carayon, S. Brustlein, A. Baude, R. Cossart, and P. P. Lenck-Santini. 2025. "GABAergic Neurons Are Major Contributors of Network Inhibition in the Neonatal Hippocampus In-Vivo." *bioRxiv*. https://doi.org/10.1101/2025.04.26.650764.

Murata, Y., and M. T. Colonnese. 2020. "GABAergic Interneurons Excite Neonatal Hippocampus in Vivo." *Science Advances* 6: eaba1430. https://doi.org/10.1126/sciadv.aba1430.

Papatheodoropoulos, C. 2010. "Patterned Activation of Hippocampal Network (~10 Hz) During in Vitro Sharp Wave-Ripples." *Neuroscience* 168: 429–442. https://doi.org/10.1016/j.neuroscience.2010.03.058.

Papatheodoropoulos, C., and G. Kostopoulos. 2002. "Spontaneous GABAA-Dependent Synchronous Periodic Activity in Adult Rat Ventral Hippocampal Slices." *Neuroscience Letters* 319: 17–20. https://doi.org/10.1016/S0304-3940(01)02505-8.

Peinado, A. 2001. "Immature Neocortical Neurons Exist as Extensive Syncitialnetworks Linked by Dendrodendritic Electrical Connections." *Journal of Neurophysiology* 85: 620–629.

Pfeffer, C. K., V. Stein, D. J. Keating, et al. 2009. "NKCC1-Dependent GABAergic Excitation Drives Synaptic Network Maturation During Early Hippocampal Development." *Journal of Neuroscience* 29: 3419–3430. https://doi.org/10.1523/JNEUROSCI.1377-08.2009.

Pochinok, I., T. M. Stöber, J. Triesch, M. Chini, and I. L. Hanganu-Opatz. 2024. "A Developmental Increase of Inhibition Promotes the Emergence of Hippocampal Ripples." *Nature Communications* 15: 738. https://doi.org/10.1038/s41467-024-44983-z.

Schlingloff, D., S. Káli, T. F. Freund, N. Hájos, and A. I. Gulyás. 2014. "Mechanisms of Sharp Wave Initiation and Ripple Generation." *Journal of Neuroscience* 34: 11385–11398. https://doi.org/10.1523/JNEUROSCI.0867-14.2014.

Strata, F., M. Atzori, M. Molnar, G. Ugolini, F. Tempia, and E. Cherubini. 1997. "A Pacemaker Current in Dye-Coupled Hilar Interneurons Contributes to the Generation of Giant GABAergic Potentials in Developing Hippocampus." *Journal of Neuroscience* 17: 1435–1446. https://doi.org/10.1523/JNEUROSCI.17-04-01435.1997.

Sullivan, D., J. Csicsvari, K. Mizuseki, S. Montgomery, K. Diba, and G. Buzsaki. 2011. "Relationships Between Hippocampal Sharp Waves, Ripples, and Fast Gamma Oscillation: Influence of Dentate and Entorhinal Cortical Activity." *Journal of Neuroscience* 31: 8605–8616. https://doi.org/10.1523/JNEUROSCI.0294-11.2011.

Valeeva, G., A. Abdullin, R. Tyzio, et al. 2010. "Temporal Coding at the Immature Depolarizing Gabaergic Synapse." *Frontiers in Cellular Neuroscience* 4: 17. https://doi.org/10.3389/fncel.2010.00017.

Valeeva, G., S. Janackova, A. Nasretdinov, et al. 2019. "Emergence of Coordinated Activity in the Developing Entorhinal–Hippocampal Network." *Cerebral Cortex* 29: 906–920. https://doi.org/10.1093/cercor/bhy309.

Valeeva, G., A. Nasretdinov, V. Rychkova, and R. Khazipov. 2019. "Bilateral Synchronization of Hippocampal Early Sharp Waves in Neonatal Rats." *Frontiers in Cellular Neuroscience* 13: 29. https://doi.org/10.3389/fncel.2019.00029.

Valeeva, G., T. Tressard, M. Mukhtarov, A. Baude, and R. Khazipov. 2016. "An Optogenetic Approach for Investigation of Excitatory and Inhibitory Network GABA Actions in Mice Expressing Channelrhodopsin-2 in GABAergic Neurons." *Journal of Neuroscience* 36: 5961–5973. https://doi.org/10.1523/JNEUROSCI.3482-15.2016.

Valiullina, F., D. Akhmetshina, A. Nasretdinov, et al. 2016. "Developmental Changes in Electrophysiological Propertiesand a Transition From Electrical to Chemical Coupling Between Excitatory Layer 4 Neurons in the Rat Barrel Cortex." *Frontiers in Neural Circuits* 10: 1. https://doi.org/10.3389/fncir.2016.00001.

Vinokurova, D., A. V. Zakharov, J. Lebedeva, et al. 2018. "Pharmacodynamics of the Glutamate Receptor Antagonists in the Rat Barrel Cortex." *Frontiers in Pharmacology* 9: 698. https://doi.org/10.3389/fphar.2018.00698.

Voronin, L. L., and E. Cherubini. 2004. "'Deaf, Mute and Whispering' Silent Synapses: Their Role in Synaptic Plasticity." *Journal of Physiology* 557: 3–12. https://doi.org/10.1113/jphysiol.2003.058966.

Weir, K., O. Blanquie, W. Kilb, H. J. Luhmann, and A. Sinning. 2015. "Comparison of Spike Parameters From Optically Identified GABAergic and Glutamatergic Neurons in Sparse Cortical Cultures." *Frontiers in Cellular Neuroscience* 8: 460. https://doi.org/10.3389/fncel.2014.00460.

Wu, C., M. N. Asl, J. Gillis, F. K. Skinner, and L. Zhang. 2005. "An in Vitro Model of Hippocampal Sharp Waves: Regional Initiation and Intracellular Correlates." *Journal of Neurophysiology* 94: 741–753. https://doi.org/10.1152/jn.00086.2005.

Ylinen, A., A. Bragin, Z. Nadasdy, et al. 1995. "Sharp Wave-Associated High-Frequency Oscillation (200 Hz) in the Intact Hippocampus: Network and Intracellular Mechanisms." *Journal of Neuroscience* 15: 30–46. https://doi.org/10.1523/JNEUROSCI.15-01-00030.1995.

Yuste, R., A. Peinado, and L. C. Katz. 1992. "Neuronal Domains in Developing Neocortex." *Science* 257: 665–669. https://doi.org/10.1126/science.1496379.